

Toward a Unified Approach to the Crystal Chemistry of Aurivillius-Type Compounds

II. $\text{Bi}_7\text{Ti}_4\text{NbO}_{21}$, a Case Study

Ph. Boullay,¹ G. Trolliard, and D. Mercurio

Laboratoire de Sciences des Procédés Céramiques et Traitements de Surface (CNRS UMR6638), Université de Limoges, 123 Avenue Albert Thomas, F-87060 Limoges Cedex, France

and

J. M. Perez-Mato and L. Elcoro

Departamento de Física de la Materia Condensada, Facultad de Ciencias, Universidad del País Vasco, Apdo. 664, E-48080 Bilbao, Spain

Received July 24, 2001; in revised form October 17, 2001; accepted December 3, 2001

In part I of this paper, a generalized structural model of Aurivillius-type compounds has been presented using a 4D superspace group analysis where Aurivillius structures are considered as cation-deficient perovskites with the general formula $AB_{1-x}O_3$. Being essentially composition independent, the model is valid for any Aurivillius-type compounds where x is the only composition-dependent parameter. For any composition, the conventional space groups can be easily derived from a unique superspace group. In this second part, a practical example of a structural refinement using the superspace approach is presented for the compound $\text{Bi}_7\text{Ti}_4\text{NbO}_{21}$ and compared with a conventional 3D refinement. Similarities with other compositionally flexible systems are discussed. © 2002

Elsevier Science (USA)

Key Words: Aurivillius phases; intergrowth compounds; modulated structures.

1. INTRODUCTION

The so-called Aurivillius phases (1) are a family of layered bismuth oxides usually described as resulting from the regular stacking of $[\text{M}_2\text{O}_2]$ slabs and perovskite-like $[\text{A}_{n-1}\text{B}_n\text{O}_{3n+1}]^{2-}$ blocks. The integer n corresponds to the number of sheets of corner-sharing BO_6 octahedra forming the perovskite blocks where the A -site can be occupied by large 12-fold-coordinated cations such as Na^+ , K^+ , Ca^{2+} , Sr^{2+} , Ba^{2+} , Pb^{2+} , Bi^{3+} , or Ln^{3+} , and the B -site by 6-fold-

coordinated cations such as Fe^{3+} , Cr^{3+} , Ti^{4+} , Nb^{5+} , or W^{6+} . While the perovskite blocks offer large possibilities in terms of compositional flexibility, the cation sites in the interleaved $[\text{M}_2\text{O}_2]$ slabs are almost exclusively occupied by Bi^{3+} cations forming $[\text{Bi}_2\text{O}_2]^{2+}$ slabs. Besides the simple members, which have been reported for n values up to 5, various ordered intergrowths of Aurivillius phases have been prepared as macroscopic pure phases.

In the first part of the present paper (2), we have investigated the possibility of forming ordered intergrowths of Aurivillius phases with long period within the pseudo-binary system $\text{Bi}_3\text{TiNbO}_9\text{--Bi}_4\text{Ti}_3\text{O}_{12}$. We have shown using electron microscopy that diffraction patterns of such intergrowths are not necessarily, at least locally, restricted to commensurate superstructure values but can vary more or less continuously. Following a recent series of papers [see (3–5) as examples] showing how compounds exhibiting a composition-dependent series of long period structures (LPS) can be described within a single model using the superspace group approach, we have established (2) an essentially composition-independent structural model valid for any particular member of the Aurivillius family. Only the modulation wave-vector and the composition-dependent width of the crenel occupational domains (further denoted AD for atomic domains) change with composition.

In this 4D superspace approach, the ferroelectric Aurivillius-type compounds are considered as B -site cation-deficient perovskites with the generalized formula $AB_{1-x}O_3$. The construction of the superspace model can be

¹To whom correspondence should be addressed. Fax: +33 5 55 45 72 70. E-mail: philippe.boullay@unilim.fr.

understood starting from an orthorhombic nonmodulated perovskite ABO_3 [see the first part of this paper (2) for details]. We have shown how the introduction of a modulation vector in the form $\mathbf{q} = x \cdot \mathbf{c}^*$ generates the occurrence of x vacancies in the B -site of the perovskite. By construction, for a given x , the sequence of B vacancies resulting from the model corresponds to a uniform sequence where the vacancies tend to be separated as much as possible. Based on this model, the ferroelectric Aurivillius-type compounds can be described using the unique superspace group $X2cm(00\gamma)000$ [see Table 1 of Part I (2) for a complete definition of the superspace group including the centering translations]. For a given rational composition x , the conventional 3D space groups can be derived from the superspace group.

In this second part of the paper we will present an experimental application where the 4D superspace approach is used in the structure refinement of the intergrowth compound $\text{Bi}_7\text{Ti}_4\text{NbO}_{21}$, which corresponds to a case $x = 2/7$ considering the formulation $\text{Bi}(\text{Ti},\text{Nb})_{1-x}\text{O}_3$. The results of the refinement and the relevance of the proposed model will be discussed.

2. EXPERIMENTAL

2.1. Synthesis

Single crystals were grown using the flux method in Bi_2O_3 excess (6). Bi_2O_3 and $\text{Bi}_7\text{Ti}_4\text{NbO}_{21}$ powders are mixed in 4:1 molar proportions in a covered platinum crucible. The following thermal treatment was applied: heating to 1200°C at $300^\circ\text{C}/\text{h}$, annealing at 1200°C for 5 h, cooling to 700°C at $5^\circ\text{C}/\text{h}$, and finally cooling to room temperature. Transparent crystals in the form of thin platelets were extracted from the solidified materials using hydrochloric acid and then washed in hot water.

2.2. X-Ray Diffraction Data Measurements

X-ray diffraction experiments were conducted on a trapezoidal flat crystal ($420 \times 220 \times 40 \mu\text{m}^3$). It was obtained by selecting and cutting under polarized light a ferroelectric domain in a thin crystalline lamella. A total of

2550 reflections were collected using a Siemens P4 four-circle automatic diffractometer using graphite-monochromatized $\text{MoK}\alpha$. They were corrected for absorption effects by a ψ -scan method (XEMP program, LAMINA option) (7).

3. REFINEMENT DETAILS OF AN $X=2/7$ CASE

The structure refinement was carried out by using the software package JANA2000 (8) taking advantage of its specific tools developed for the 4D treatment of 3D commensurate long period structures. The experimental data used for this refinement are the same as the ones used in our previous structure refinement with conventional 3D methods (9) (see Section 2.2 and Table 1 for further details regarding the data collection).

Before starting the refinement, it is important to have in mind some of the assumptions we made to build the layer model, i.e.:

- The layer model is essentially composition independent.
- The atomic domains (further denoted AD) representing the atoms in the superspace (see Fig. la) are discontinuous and are defined using crenel functions (for Ti, Bi, and O(1)).
- The atomic displacements along the stacking direction can be modeled to a first approximation using sawtooth functions (for Ti, Bi, and O(1)) as illustrated in Fig. la.
- The refined structure should be a slightly perturbed solution of the one obtained using only sawtooth functions.

The different steps of the refinement will have to follow these assumptions and, as it will be shown later, the last point appears to us of importance to conclude successfully the refinement and avoid “unstable” solution. Also, in the above composition-independent layer model, no attention has been paid to the chemical nature of the cations located at the A - and B -sites. Hence in our practical case, we will first neglect the contribution of the Nb cations.

The general starting structural parameters describing the asymmetric unit with its occupational domains are listed in Table 2. The thermal motion factors are all fixed to a value corresponding to $U_{\text{iso}} = 0.02$. In our condensed notation, $\text{Bi}_7\text{Ti}_4\text{NbO}_{21}$ corresponds to $\text{Bi}(\text{Ti},\text{Nb})_{1-x}\text{O}_3$ where the value of the modulation vector is related to the B -site deficiency through the relation $\mathbf{q} = x \cdot \mathbf{c}^*$ with $x = 2/7$. Following Table 2 of Part I (2), for $x = \text{even/odd}$ and $\phi = 0$, the corresponding 3D structure will have the space group $I2cm$ ($n^\circ 46$). The number of refinable parameters for this space group is listed in Table 3. Due to the polar nature of the structure, the parameter representing the average position $x[\text{Bi}]$ is fixed to zero.

TABLE 1
Crystal Data for $\text{Bi}_7\text{Ti}_4\text{NbO}_{21}/\text{Bi}(\text{Ti}_{4/7}\text{Nb}_{1/7})\text{O}_3$
(Data Collection Done in the Supercell)

Formula	$\text{Bi}_7\text{Ti}_4\text{NbO}_{21}$	Z, density ($\text{g}\cdot\text{cm}^{-3}$)	4, 8.11
Wavelength (\AA)	0.71073	Monochromator	Graphite
	($\text{MoK}\alpha$)		
θ range ($^\circ$)	5.36–30	h, k, l range	$\pm 7, \pm 7, \pm 80$
Crystal size (μm^3)	$420 \times 220 \times 40$	$F(000)$	3512
Reflections measured	2438	Reflections unique	1293
$R_{\text{int}} [I > 3\sigma(I)]/\text{all}$	0.0274		

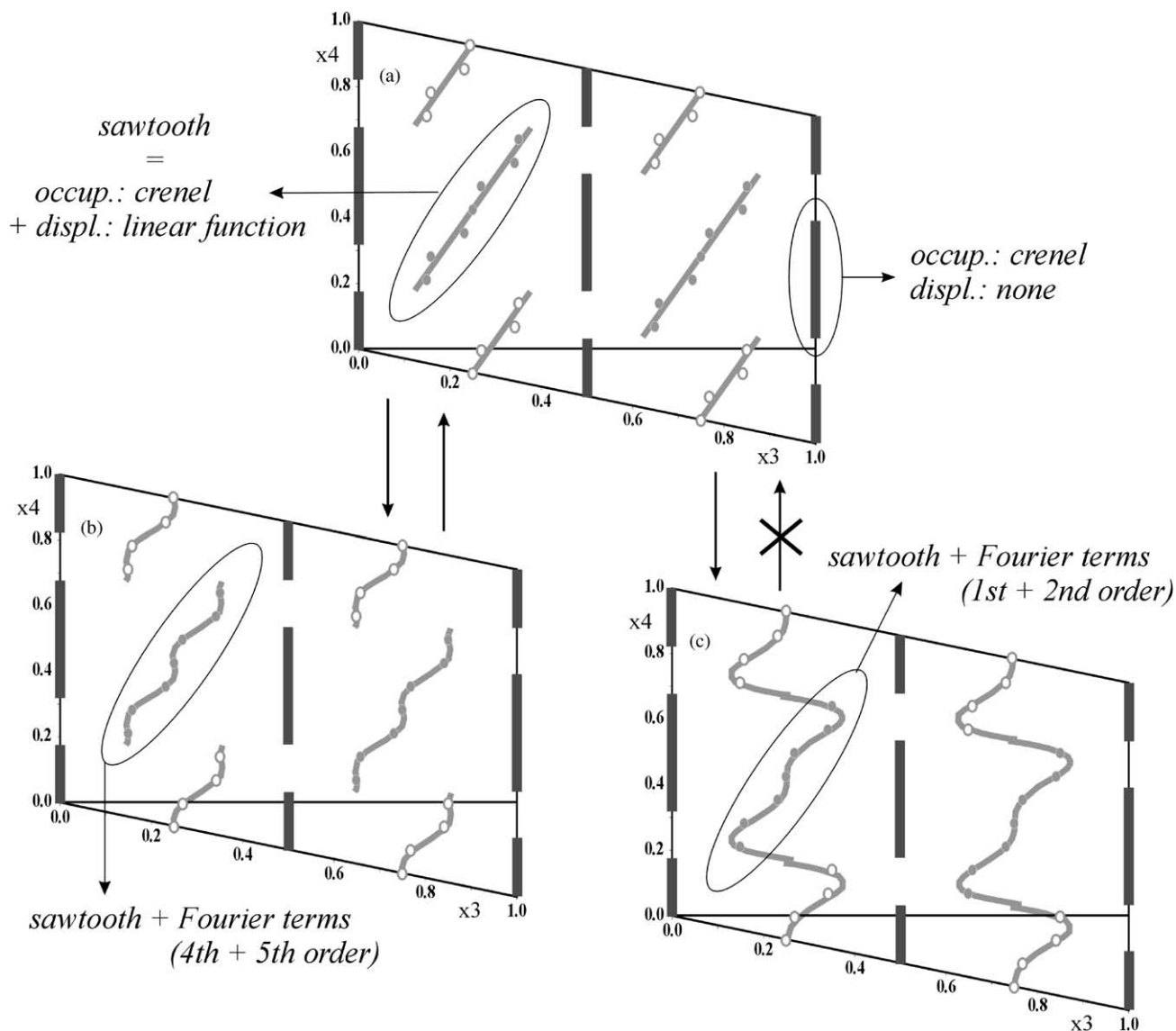


FIG. 1. Illustration of the method used to refine the displacive modulation for Bi atoms. (a) AD of the cationic sites Bi and Ti have occupations limited by crenel functions. In the very first stage of the refinement, a prime displacive modulation is introduced for Bi using a sawtooth function. (b) In the refinement of the displacive modulation, the sawtooth function is smoothly modified by introducing Fourier terms of high order. This solution is reversible. (c) In the refinement of the displacive modulation, the sawtooth function is strongly perturbed by introducing Fourier terms of low order. This solution is not reversible.

As the Bi atoms dominate the X-ray scattering, the first step of the refinement consists to fix the AD representing the Bi displacements. After a first refinement of the scale factor and the average positions $x[\text{Ti}]$ and $y[\text{Bi}]$, we introduce the sawtooth function for the displacements along the stacking direction z leaving the x and y directions unaffected by modulation. By doing so we obtain the AD depicted in Fig. 1a with an R_{obs} around 36%. Then, as indicated in Table 3, two supplementary parameters can be added to describe the displacements along the z direction. The choice of how these parameters shall be introduced will play a major role on the following steps of the refinement. If we choose to add the supplementary

modulation using terms of the first and second order in the Fourier series, the system converges to a value R_{obs} around 19% with the AD represented in Fig. 1c. Looking at the amplitudes of the refined parameters, we observe that they are all very strong and that the added modulation represents a strong perturbation of the sawtooth function first introduced. Compared to its initial value, the slope of the sawtooth function happens to be multiplied by a factor of 20 and have an opposite sign. As a result, if we suppress the two extra parameters we do not recover the initial configuration displayed in Fig. 1a. Alternatively, if we try to fix the slope of the sawtooth and refine only the two extra parameters, it is not possible to obtain a suitable

TABLE 2
General Structural Parameters in the Superspace Description of the Polar Common Structure with Superspace Group $X2cm(00x)000^a$

Element	x_1	x_2	x_3	x_4	Δ	Point symmetry of the average position	Displacive modulation
Bi	$\underline{0}$	$\underline{0}$	$\frac{1}{4}$	$\frac{1}{2}$	$\frac{1}{2}$	11m	$(x_s(x_4), y_s(x_4), z_a(x_4))$
Ti/Nb	$\underline{0}$	$\underline{0}$	$\underline{0}$	$\underline{0}$	$(1-x)/2$	211	$(x_s(x_4), y_a(x_4), z_a(x_4))$
O(1)	$\underline{0}$	$\underline{0}$	$\frac{1}{4}$	$\underline{0}$	$\frac{1}{2}$	11m	$(x_s(x_4), y_s(x_4), z_a(x_4))$
O(2)	$\underline{\frac{1}{4}}$	$\underline{\frac{1}{4}}$	$\underline{0}$	—	—	1m1	$(x^{even}(x_4), y^{odd}(x_4), z^{even}(x_4))$

^a x_4 and Δ , if given, represent the center and width of the crenel function (10) describing the corresponding occupation atomic domain. Underlined parameters indicate positions not restricted by symmetry. In the last column, a and s stand for antisymmetric and symmetric functions, respectively. Even (odd) superscripts indicate that only even (odd) terms are present in the Fourier expansion series.

representation of the AD. Now if we consider that displacements along the z direction should be a slightly perturbed solution of the one obtained using the sawtooth function, we can make the choice to refine the supplementary modulation using terms of higher order which will have a smoother effect. We refine Fourier terms of the fourth and fifth order obtaining a convergence to a value R_{obs} around 19% with the AD represented in Fig. 1b. Under these conditions the three parameters (including the sawtooth) describing the displacements along the z direction can be refined simultaneously without strong modification of the main modulation represented by the sawtooth. The amplitude of the added terms is small and, when suppressed, the initial configuration of Fig. 1a is recovered. Notice that both solutions allow us to describe properly the displacements along the z direction (see significant points superimposed onto the two AD in Figs. 1b and 1c) but only the last one using terms of high order in the Fourier series will allow us to reach a stable solution in the final steps of the refinement. Also this solution is in perfect coherence with our assumption. The possibility of restricting to zero the lower Fourier terms and using only the higher ones plus the sawtooth function is related with the fact that the Fourier terms are not orthogonal to the sawtooths, especially those of lower order, causing a strong

correlation in the refinement. Even Fourier terms when limited to the crenel intervals are not orthogonal and may cause undesired correlations in the refined parameters (10). Fixing the first Fourier terms to zero reduces redundancies in the used basis of functions and palliates this problem in a simple efficient form. A more systematic and rigorous procedure would be to construct and use for the modulations description a set of orthogonalized functions within the crenel interval as proposed in (10), but the use of the sawtooth function makes this method rather ineffective.

The next steps of the refinement were conducted using the same strategy for the modulation along the z direction in case of sites defined by discontinuous AD (i.e., all except O(2)). For the modulations along the x and y directions, as no sawtooth function is included in these directions, Fourier terms with lower order (second and third order) are the most relevant, while the higher ones can be fixed to zero as they proved to be not significant in the refinement. Similarly, for the continuously defined O(2) site, the displacive modulation is found to be well described using low-order Fourier terms and most of the high-order Fourier terms, theoretically possible, can be neglected (see Table 4). Using such selection of the Fourier terms, we obtain a lowering of refined parameters compared to the conventional 3D refinement (see Table 3). Once the displacement modulations have been fixed for all atoms, we obtain along the z direction the AD represented in Fig. 2. At this point the R_{obs} value is about 7.5% using average anisotropic thermal parameters for the Bi and Ti atomic positions and an average isotropic thermal parameter for O(1) and O(2) atomic positions. A twin was also introduced to account for 90° oriented domains in the x_0y plane.

Up to this stage of the refinement, no attention has been paid to eventual mixed occupancy of the cationic sites. This possibility can be taken into account by JANA2000 that has been recently adapted for this purpose. Two atomic positions, for Ti and Nb atoms, with equal positional and thermal parameters are used. The relative occupancy of

TABLE 3
Number of Position Parameters Used in the 4D Commensurate Refinement Referred to an Equivalent 3D Refinement (Corresponds to the Maximal Number of Parameters That Can Be Refined in the 4D Approach for the Case $x=2/7$)

Site	3D refinement			4D refinement		
	x_1	x_2	x_3	x_1	x_2	x_3
Bi	3	4	3	3	$\underline{3}$	3
Ti/Nb	3	2	2	$\underline{2}$	$\underline{2}$	2
O(1)	4	4	3	$\underline{2}$	$\underline{2}$	$\underline{2}$
O(2)	7	7	7	$\underline{5}$	$\underline{4}$	$\underline{5}$

TABLE 4
X*2*cm* (00*x*)000 with *a* = 5.442(1) Å, *b* = 5.404(1) Å, *c* = 8.2843(17) Å, and *q* = 2/7*c*

General Parameters and Reliability Factors

Formula: Bi(Ti _{4/7} Nb _{1/7})O ₃	Z: 28	Volume (Å ³): 243.6(1)
Number of observed reflections (main /1 st /2 nd /3 rd / and more): 165/321/343/354		
Extinction correction: Isotropic, type I, 0.0095(4)		
<i>R</i> indices [<i>I</i> > 3σ(<i>I</i>)/all data]	<i>R</i> = 0.044/0.0519	w <i>R</i> = 0.0425/0.0427
Main reflections	<i>R</i> = 0.0521/0.0638	w <i>R</i> = 0.0547/0.0548
Sat. order 1	<i>R</i> = 0.0428/0.0524	w <i>R</i> = 0.0341/0.0344
Sat. order 2	<i>R</i> = 0.0443/0.0514	w <i>R</i> = 0.0424/0.0425
Sat. order 3 and more	<i>R</i> = 0.0398/0.0443	w <i>R</i> = 0.0421/0.0423

Fractional Coordinates and Thermal Parameters (Å²) of the Average Structure

Site	<i>x</i>	<i>y</i>	<i>z</i>	<i>U</i> _{iso} / <i>U</i> _{eq}
Bi	0 ^a	-0.01036(12)	0.25	0.0194(2)
Ti/Nb	-0.0367(5)	0	0	0.0045(7)
O(1)	-0.054(2)	-0.072(2)	0.25	0.024(2)
O(2)	0.2125(19)	0.25	0.0187(12)	0.0157(16)

Site	<i>U</i> ₁₁	<i>U</i> ₂₂	<i>U</i> ₃₃	<i>U</i> ₁₂	<i>U</i> ₁₃	<i>U</i> ₂₃
Bi	0.0197(4)	0.0179(3)	0.0205(3)	-0.0031(7)	0	0
Ti/Nb	0.0033(15)	0.0066(12)	0.0037(9)	0	0	0.0009(11)

Parameters for the Sawtooth Functions

Site	<i>x</i> ₄	Δ	Slope <i>z</i> ^b
Bi	1/2	1/2	0.12536(12)
Ti/Nb	0	0.357143	0.0247(5)
O(1)	0	1/2	-0.050(3)

Displacive Fourier Terms

		Bi		Ti/Nb		O(1)		O(2)	
		sin	cos	sin	cos	sin	cos	sin	cos
<i>x</i>	1	0	—	0	—	0	—	—	—
<i>y</i>	1	0	—	—	0	0	—	0.008(2)	0.021(3)
<i>z</i>	1	—	0	—	0	—	0	—	—
<i>x</i>	2	0.0035(3)	—	0	—	-0.032(3)	—	-0.026(2)	-0.036(2)
<i>y</i>	2	0	—	—	0	-0.024(3)	—	—	—
<i>z</i>	2	—	0	—	0	—	0	0.0175(17)	-0.0270(16)
<i>x</i>	3	0	—	0	—	0	—	—	—
<i>y</i>	3	-0.0057(3)	—	—	0	0	—	0	0.030(2)
<i>z</i>	3	—	0	—	0	—	0	—	—
<i>x</i>	4	-0.0045(3)	—	0	—	0	—	0.015(2)	-0.008(3)
<i>y</i>	4	0.0088(6)	—	—	-0.0018(15)	0	—	—	—
<i>z</i>	4	—	-0.00227(11)	—	0	—	-0.007(2)	-0.0044(16)	0
<i>x</i>	5	0	—	0.0055(9)	—	0	—	—	—
<i>y</i>	5	0.0102(5)	—	—	0.0023(14)	0	—	0	0
<i>z</i>	5	—	0.01952(10)	—	0.0032(3)	—	0	—	—
<i>x</i>	6	—	—	—	—	—	—	0	0
<i>y</i>	6	—	—	—	—	—	—	—	—
<i>z</i>	6	—	—	—	—	—	—	0	0.0124(12)

TABLE 4—Continued

		Thermal Parameters Fourier Terms					
		Bi atomic site					
		U_{11}	U_{22}	U_{33}	U_{12}	U_{13}	U_{23}
sin	1	—	—	—	—	0	0
cos	1	0	0	0	0	—	—
sin	2	—	—	—	—	0	0
cos	2	0.0023(6)	0	0	0	—	—
sin	3	—	—	—	—	0	0
cos	3	0.0054(6)	−0.0032(3)	0	0	—	—
sin	4	—	—	—	—	−0.023(4)	0.012(2)
cos	4	0	0	0.0175(7)	0	—	—
sin	5	—	—	—	—	−0.053(8)	0.029(4)
cos	5	0	0	0.0197(7)	0.0024(11)	—	—
sin	6	—	—	—	—	−0.048(7)	0.025(4)
con	6	0	0	0.0114(4)	0.0029(11)	—	—

^aFixed coordinate.

^b x and y are set to zero.

these two atomic species can then be adjusted by using a supplementary modulation wave. Notice that by doing so, the actual location of the different chemical species inside the structure can be found without any prime assumption. Regarding the thermal parameters, modulations of the U_{ij} anisotropic thermal parameters were added for Bi atoms and the selection of dominant Fourier terms was applied as for the displacement modulations. For the mixed Ti/Nb atomic position, only nonmodulated average U_{ij} anisotropic thermal parameters were used while average U_{iso} parameters were refined for the oxygen positions O(1) and O(2). In the very last stage of the refinement an extinction parameter (type I) has been added leading to the structural parameters and the final reliability factors displayed in Table 4.

4. RESULTS AND DISCUSSION

4.1. 3D Long Period versus 4D Commensurate Description

In order to compare the result of this refinement with our previous conventional 3D study (9), the 4D commensurate modulated structure was converted to the 3D supercell structure. Anisotropic and isotropic thermal parameter, for B and O atomic sites respectively, were refined independently. In Table 5, the 3D structure obtained from the 4D model is displayed together with the reliability factors and the resulting interatomic distances. It is noticeable that the results are in good agreement with the ones obtained from our previous 3D study (9). The examination of the occupancy obtained for the *B*-sites with mixed occupancy indicates, as shown in our previous work, that the atomic position noted Ti/Nb(3) in Table 5 is the only one significantly occupied by Nb atoms.

A drawing of the corresponding 3D structure ($y0z$ projection) is given in Fig. 3. Along the z direction (stacking direction), the structure of $\text{Bi}_7\text{Ti}_4\text{NbO}_{21}$ corresponds to the regular intergrowth of half a unit cell of $\text{Bi}_3\text{TiNbO}_9$ and half a unit cell of $\text{Bi}_4\text{Ti}_4\text{O}_{12}$. In turn, these two parts can be seen respectively as double and triple perovskite blocks intergrown with intermediate $[\text{Bi}_2\text{O}_2]$ slabs. Alternatively, the $\text{Bi}_7\text{Ti}_4\text{NbO}_{21}$ structure can be seen as a regular stacking of a triple and a quadruple perovskite shifted with respect to each other by a $1/2\mathbf{a}$ translation, which generates the occurrence of *B*-site vacancies resulting in the existence of $[\text{Bi}_2\text{O}_2]$ slabs in the stacking. This last description is the one we used to create our model and also appears as the one in best agreement with the observations made in ED (see Part I of this paper), where the electron diffraction patterns (EDP) of the compounds $\text{Bi}_3\text{TiNbO}_9$ and $\text{Bi}_4\text{Ti}_3\text{O}_{12}$ indicate respectively a perovskite supercell of order 3 and 4 along the z direction.

Within this publication, we would like to emphasise the correspondence between both 3D and 4D representations. Directed toward readers less familiar with the 4D superspace representation, it is important to explain in detail how Fig. 2 should be interpreted to obtain the z coordinates of the atoms in the 3D space. This is done by observing the z coordinates of the corresponding modulation functions at successive cuts of the 4D space (separated by $2/7$ and perpendicular to the x_4 direction). Considering the value $x = 2/7 = \text{even/odd}$ of the modulation vector, the 3D space group $I2cm$ corresponds to a choice of the origin of the first section at 0 ($\phi = 0$), or the equivalent [see Table 2 of Part I (2)]. Under this choice, the origin of the cell represented in Fig. 2 is on the glide plane of the space group $I2cm$ and defines the origin of the atomic sequences in the middle of the $\text{Bi}_4\text{Ti}_3\text{O}_{12}$ part of the structure. Starting from this origin and moving to the right of the

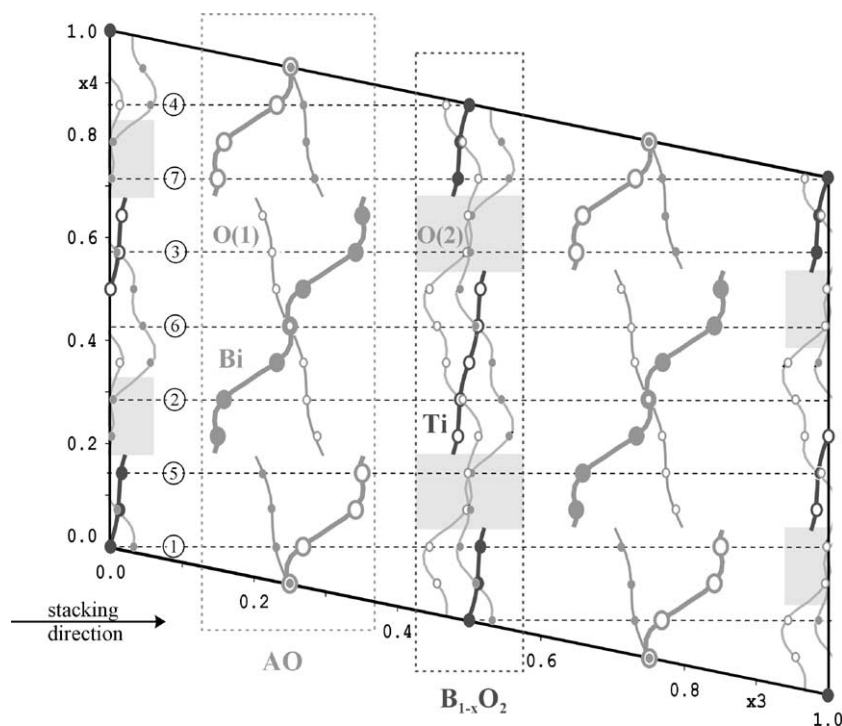


FIG. 2. x_3 - x_4 section of the 4D structural model obtained from the refinement of an $x = 2/7$ case. The z coordinates of the equivalent 3D supercell structure are obtained by successive cuts perpendicular to the x_4 direction (dashed lines taken in order of numerotation). Atomic domains are represented by slopes on which the points corresponding to the position of an atom in the physical 3D space are represented. Full and empty circles of the same size are used to indicate equivalent AD but with different locations along the $x_1 = x$ and $x_2 = y$ directions.

horizontal section gives the sequence of the different atoms in the stacking sequence and the value Δz between two successive atoms. At the end of the section, one goes to the next which is located at $x_4 + 2/7$ (modulo 1) and this until we come back to the first section at $x_4 = 0$, i.e., after seven steps. Moving from the left to the right in Fig. 2 corresponds to going up along the stacking direction in Fig. 3. Thus for the first section crossing $x_4 = 0$, we get the succession Ti-O(2)/O(1)-Bi/O(2)-O(2)-Ti/O(1)-Bi/O(2)- and then we continue with the section $x_4 = 2/7$ —O(2)/Bi-O(1)/Ti-O(2)-O(2)/... and so on. This corresponds to the column parallel to (x_0z) and noted 1 in Fig. 3. As the layer sequence in the adjacent sheet noted 2 equivalent to the one in column 1 but shifted, this column is obtained in a similar way by applying symmetry operations to the column 1. Notice that Fig. 2 describes only the coordinates along the z direction and to get a strict correspondence with Fig. 3, one should do a similar reading on an x_2 - x_4 4D representation in order to obtain the coordinates along the y direction. A program like JANA2000, which allows us to go directly from the 4D commensurate structure to the 3D long period supercell, automatically does such readings.

Lastly notice that one could estimate the equivalence of the two models just by checking that the points corre-

sponding to an atomic position in the previous 3D model fall onto the AD obtained in the 4D refinement. This was done in Fig. 2, where the direct comparison between the two methods clearly demonstrates this equivalence.

4.2. Structural Features beneath the 4D Representation

The double continuous atomic domains for O(2) that can be seen in Fig. 2 are the 4D transposition of the octahedra tilting observed in Aurivillius low-temperature phases. It is noticeable that the O(2) atoms located in the shear plane (O_2 plane) are not affected by any rotation and their positions along the c direction are equivalent to those of the ideal model. It appears that one may distinguish two types of O(2) atoms, the ones belonging to BO_2 planes and the ones belonging to O_2 planes. Notice that the continuous O(2) atomic domains could be split into two limited domains using crenel functions to separate O(2) atoms located within the $[Bi_2O_2]$ slab from the others. Such splitting was not used since it proves to be not necessary. Indeed, large shifts from the average position can perfectly be taken into account by the 4D refinement.

Figure 6c of Part I (2) represents an ideal Aurivillius compound $AB_{1-x}O_3$ with B -site vacancies after the introduction of a modulation vector $\mathbf{q} = x \cdot \mathbf{c}^*$. After the

4D refinement, the real representation of the structure corresponding to the modulation vector $\mathbf{q} = 2/7 \cdot \mathbf{c}^*$ is given in Fig. 2. In this representation, atomic displacements have been refined and we can notice that in contrast to the ideal model presented in Part I, the atomic domains are no longer parallel to the x_4 direction. More precisely, it appears that in the real 4D structure the atomic domains of cations and oxygens are tilted in opposite ways (Fig. 2). While in the ideal model, cations and oxygens respectively in the BO_2 and AO sheets had the same coordinates z , this opposite evolution of cationic and anionic domains is indicative first of an expansion of the cationic sublattice and second of a compression of the anionic sublattice along the z direction. In Fig. 2, this phenomenon is especially obvious for the AO layers where the modulation functions of the oxygen O(1) and Bi cations form a crosslike pattern.

Such a structural reorganization can be understood as a natural consequence of the fact that while there exist fewer cationic layers (six cationic layers versus seven anionic layers in Fig. 3), both cationic and anionic sublattices should have the same global periodicity along the z direction. As a result, such crosslike patterns are typical for $AB_{1-x}O_3$ -type compounds [see (3, 4) as an example in hexagonal perovskites] as well as $A_{1-x}BO_3$ -type compounds. In the corresponding 3D drawing of the structure displayed in Fig. 3, this corresponds to a progressive shift along the z direction of the A cations from the center of the cuboctahedral site of the perovskite toward the shear planes (O_2 planes) in order to compensate the cationic deficit induced by the existence of the B -site vacancies. The closer the A cation is to a O_2 plane, the larger will be the shift toward this plane. Nonetheless, one can notice that B

TABLE 5
***I*2cm (no. 46) with $a = 5.442(1)$ Å, $b = 5.404(1)$ Å, $c = 57.990(12)$ Å**

General Parameters and Reliability Factors						
Formula: $Bi_7Ti_4NbO_{21}$		Z: 4		Volume(Å ³): 1705.4(6)		
Number of observed reflections: 1183						
Extinction correction: Isotropic, type I, 0.0026(1)						
R indices [$I > 3\sigma(I)$ /all data]		R = 0.0448/0.0525		wR = 0.0434/0.0436		
Fractional Coordinates and Thermal Parameters(Å ²) of the Supercell Structure ^a						
	Wickoff	x	y	z	U_{iso}/U_{eq}	
Bi(1)	8c	0 ^b	-0.0210(3)	0.165478(19)	0.0186(3)	
Bi(2)	4b	-0.0043(8)	-0.0061(4)	3/4	0.0227(4)	
Bi(3)	8c	-0.0099(9)	0.4825(3)	0.121535(17)	0.0163(3)	
Bi(4)	8c	-0.0008(7)	0.4952(3)	0.538333(18)	0.0193(3)	
Ti(1)	4a	-0.0356(18)	0	0	0.0022(18)	
Ti(2)	8c	-0.0419(10)	0.0015(11)	0.42614(7)	0.0029(12)	
Ti/Nb(3)	8c	-0.0440(8)	0.4998(10)	0.21252(6)	0.0121(11)	
O(1a)	8c	-0.080(5)	-0.082(5)	0.0325(5)	0.033(7)	
O(1b)	8c	-0.019(7)	-0.044(4)	0.6011(4)	0.028(6)	
O(1c)	4b	-0.081(6)	0.404(6)	1/4	0.020(7)	
O(1d)	8c	-0.053(4)	0.424(4)	0.6821(3)	0.016(5)	
O(2a)	8c	0.198(5)	0.265(6)	0.0048(4)	0.028(8)	
O(2b)	8c	0.231(6)	0.246(6)	0.1429(4)	0.009(6)	
O(2c)	8c	0.155(4)	0.202(4)	0.2865(4)	0.013(4)	
O(2d)	8c	0.239(6)	0.227(8)	0.4368(4)	0.022(6)	
O(2e)	8c	0.172(4)	0.282(5)	0.5695(4)	0.013(5)	
O(2f)	8c	0.227(5)	0.279(6)	0.7211(4)	0.017(5)	
O(2g)	8c	0.250(9)	0.257(8)	0.8573(4)	0.018(6)	
	U_{11}	U_{22}	U_{33}	U_{12}	U_{13}	U_{23}
Bi(1)	0.0241(7)	0.0153(6)	0.0162(4)	-0.0018(13)	0.0042(17)	-0.0031(5)
Bi(2)	0.0168(8)	0.0215(8)	0.0300(7)	0.001(2)	—	—
Bi(3)	0.0213(5)	0.0161(6)	0.0114(3)	-0.0068(10)	-0.0057(11)	0.0027(5)
Bi(4)	0.0203(6)	0.0186(5)	0.0189(4)	-0.0036(16)	-0.0008(14)	-0.0003(5)
Ti(1)	0.000(4)	0.004(2)	0.002(2)	—	—	0.002(4)
Ti(2)	0.001(3)	0.0042(19)	0.0030(14)	0.0003(18)	0.001(2)	0.002(2)
Ti/Nb(3)	0.011(2)	0.0154(16)	0.0096(12)	0.0013(15)	-0.0008(14)	0.000(2)

TABLE 5—Continued

Interatomic Distances(Å) in the Coordination Sphere of Bi and Ti Atoms									
Ti(1)	–	O(1a)	1.95(2)	<i>x</i> 2	Bi(2)	–	O(2c)	2.52(2)	<i>x</i> 2
	–	O(2a)	1.94(3)	<i>x</i> 4		–	O(2f)	2.60(3)	<i>x</i> 2
Ti(2)	–	O(1a)	2.45(3)	<i>x</i> 1	Bi(3)	–	O(2f)	2.54(3)	<i>x</i> 2
	–	O(1b)	1.60(2)	<i>x</i> 1		–	O(1c)	2.35(3)	<i>x</i> 1
	–	O(2d)	2.05(3)	<i>x</i> 1		–	O(1c)	2.19(3)	<i>x</i> 1
	–	O(2d)	1.99(4)	<i>x</i> 1		–	O(1b)	2.92(3)	<i>x</i> 1
	–	O(2e)	1.94(2)	<i>x</i> 1		–	O(1b)	2.65(2)	<i>x</i> 1
	–	O(2e)	1.98(2)	<i>x</i> 1		–	O(2b)	2.21(3)	<i>x</i> 1
Ti/Nb(3)	–	O(2c)	1.94(2)	<i>x</i> 1	Bi(4)	–	O(2b)	2.25(3)	<i>x</i> 1
	–	O(2c)	1.97(2)	<i>x</i> 1		–	O(2g)	2.34(4)	<i>x</i> 1
	–	O(2f)	2.02(3)	<i>x</i> 1		–	O(2g)	2.33(4)	<i>x</i> 1
	–	O(2f)	1.96(3)	<i>x</i> 1		–	O(1a)	2.35(3)	<i>x</i> 1
	–	O(1c)	2.244(9)	<i>x</i> 1		–	O(1a)	2.30(3)	<i>x</i> 1
	–	O(1d)	1.81(2)	<i>x</i> 1		–	O(2a)	2.58(2)	<i>x</i> 1
Bi(1)	–	O(2b)	2.32(3)	<i>x</i> 1	–	O(2a)	2.93(2)	<i>x</i> 1	
	–	O(2b)	2.46(3)	<i>x</i> 1	–	O(2d)	2.46(2)	<i>x</i> 1	
	–	O(2g)	2.28(4)	<i>x</i> 1	–	O(2d)	2.38(3)	<i>x</i> 1	
	–	O(2g)	2.25(4)	<i>x</i> 1	–	O(2e)	2.34(2)	<i>x</i> 1	
	–	O(1d)	2.63(2)	<i>x</i> 1	–	O(2e)	2.95(2)	<i>x</i> 1	
	–	O(1d)	2.40(2)	<i>x</i> 1					

^aThe atomic positions denoted O(1–) and O(2–) represent respectively positions generated from the atomic positions O(1) and O(2) of the 4D structure.

^bFixed coordinate (polar space group).

cations are less affected by this expansion. This can be understood by the existence of oxygens in direct opposition in both the upper and lower atomic planes, which limit strongly the displacements along the *z* direction of the *B* cations. In this respect, one can notice that the Ti(2)–O(1b) distance of 1.6 Å is already very short and one can hardly expect that the *B* cations get closer from an apex of their octahedral coordination shell. In contrast, if we compare with the case of hexagonal perovskites where the *B* cations can move along the *z* direction towards a face of their octahedral coordination shell, the expansion of the cationic sublattice affects in a similar way both *A* and *B* cationic sites.

4.3. A Unified Description?

In the above discussion we have shown the equivalence between the 4D commensurate and the 3D long period description using the structure refinement of the compound Bi₇Ti₄NbO₂₁ as an example. We will now show that this 4D structural model obtained for a case $x=2/7$ is almost directly applicable to other compounds within the pseudobinary system Bi₃TiNbO₉–Bi₄Ti₃O₁₂. Taking the AD obtained from our refinement of an $x=2/7$ case, we can check their validity for the cases $x=1/4$ (Bi₄Ti₃O₁₂) and $x=1/3$ (Bi₃TiNbO₉) by adjusting the 4D model to these two cases. This is done simply by modifying the modulation wave-vector $\mathbf{q}=x\cdot\mathbf{c}^*$ and thus the width of the crenel

for the *B* atomic site (see Table 2). From this one can generate an $x3-x4$ section diagram and superimpose onto this diagram the atomic positions taken in the literature and obtained from previous 3D conventional refinement. As illustrated in Fig. 4, the points corresponding to atomic positions in the model obtained in (11) for $x=1/3$ (SG no. 36 *A2₁am*) and in (12) for $x=1/4$ (SG no. 41 *B2ab*) fall close to the AD obtained in our 4D refinement of a case $x=2/7$. This proves that the 4D description succeeds in capturing and unifying the structural features common to these Aurivillius-type compounds. Also, the description of atomic displacements using sawtooth functions appears as a good approximation.

Notice that for the case $x=1/4$, the monoclinic solution found in (13) (SG no. 7 *B1a1*) is also possible within our generalized description and, similarly to the orthorhombic solution found in (12), can also be described using our crystallographic model. In this respect, this example clearly illustrates that our description does not give a unique possibility for commensurate cases but limits the choice to three space groups (see Part I). This choice is ultimately governed by the results of the refinement of the crystallographic data.

5. CONCLUSION

We have shown that the ferroelectric Aurivillius phases of the pseudobinary system Bi₃TiNbO₉–Bi₄Ti₃O₁₂ can all

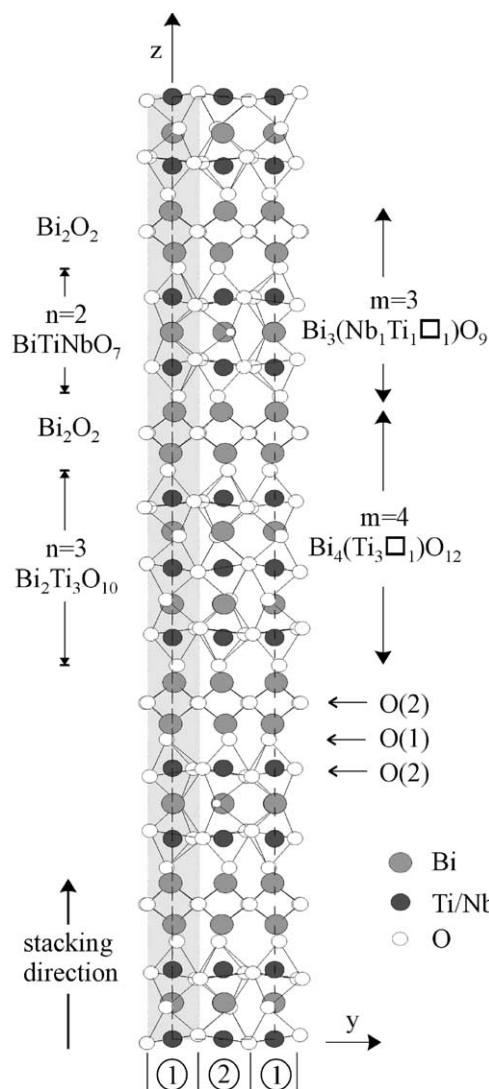


FIG. 3. $\text{Bi}_7\text{Ti}_4\text{NbO}_{21}$ structure in projection along a . Along the z direction, the different type of slabs constitutive of the structure are indicated. Depending on the type of description, the $[\text{Bi}_2\text{O}_2]$ slabs are set apart from the perovskite blocks or not. Only this last description allows us to obtain a unified description for all the Aurivillius-type structures. Along the y direction, related one to the other through symmetry operations, two types of sheets (noted 1 are 2) are found.

be described as modulated structures with a composition-dependent modulation wave-vector. The generalized model developed in (2) has been applied to the intergrowth compound $\text{Bi}_7\text{Ti}_4\text{NbO}_{21}$ and it is shown that the results of such a 4D commensurate structure refinement are entirely equivalent to a 3D long period superstructure refinement. Additionally, a comparison of several commensurate structures of different composition demonstrates that the modulation functions are strikingly composition independent.

In the usual conventional 3D crystallographic approach, the features common to the whole family of reported Aurivillius structures are blurred. The presented model, using the 4D superspace formalism, emphasizes these features. The fundamental advantage of this approach is that, using the modulated description explained above, the complexity of the structural analysis is essentially independent of the material composition and of the more or less large volume of the conventional unit cell. Hence, it can be used in the structure refinement of new or yet ill-defined long period intergrowth Aurivillius-type compounds.

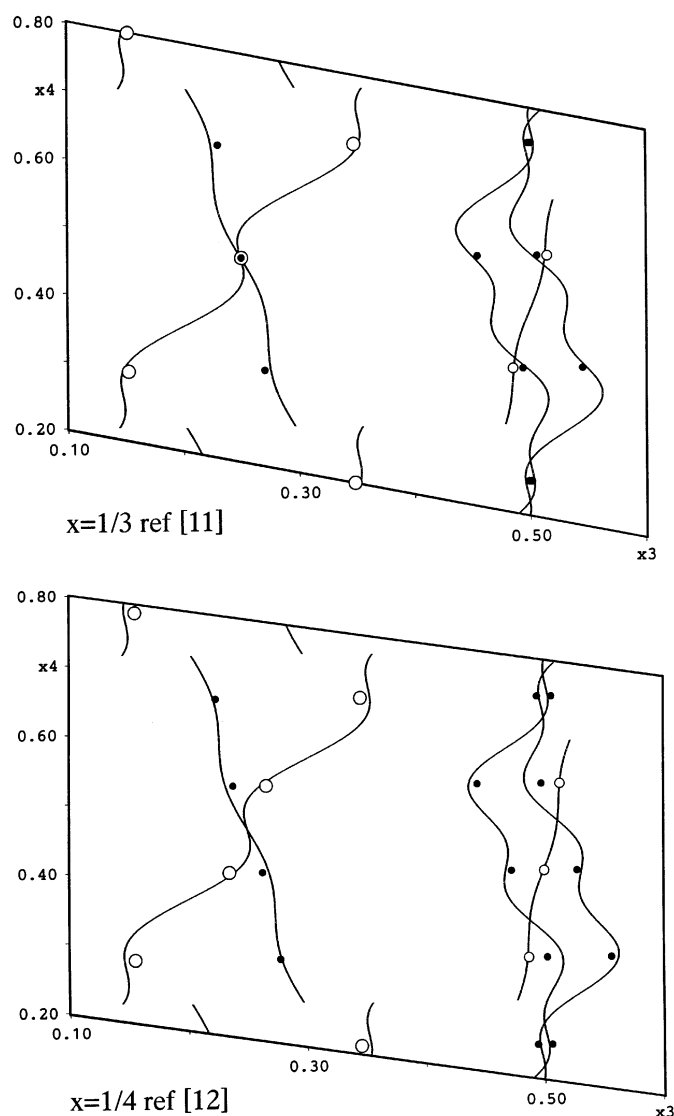


FIG. 4. Illustration of the striking independence of the modulation functions with respect to the chemical composition. The modulation functions, represented by curves in the x_3 - x_4 diagrams, and describing the layer stacking, are obtained from the refinement corresponding to the case $x=2/7$ ($\text{Bi}_7\text{Ti}_4\text{NbO}_{21}$). The atomic positions, represented by points, and corresponding to the cases $x=1/3$ ($\text{Bi}_3\text{TiNbO}_9$) and $x=1/4$ ($\text{Bi}_4\text{Ti}_3\text{O}_{12}$), are obtained from the literature (11, 12).

ACKNOWLEDGMENTS

The authors thank Dr. V. Petricek for valuable discussions and for his kindness to provide us modifications of JANA2000.

REFERENCES

1. B. Aurivillius, *Arkiv. Kemi* **1**, 463–480 and 499–512 (1949).
2. Ph. Boullay, G. Trolliard, D. Mercurio, J. M. Perez-Mato, and L. Elcoro, in this issue of *J. Solid State Chem.*
3. J. M. Perez-Mato, M. Zakhour-Nakhl, F. Weil, and J. Darriet, *J. Mater. Chem.* **9**, 2795 (1999).
4. O. Gourdon, V. Petricek, M. Dusek, P. Bezdzicka, S. Durovic, D. Gyepesova, and M. Evain, *Acta Crystallogr. B* **55**, 841 (1999).
5. L. Elcoro, J. M. Perez-Mato, and R. Withers, *Z. Kristallogr.* **215**, 727 (2000).
6. R. Maalal, R. Von der Mühl, G. Trolliard, and J. P. Mercurio, *J. Phys. Chem. Solids* **57**, 1957 (1996).
7. G. M. Sheldrick, Shelxtl-pc, version 4-1, Siemens Analytical X-ray Instr. Inc., Madison WI, 1998.
8. V. Petricek and M. Dusek, The Crystallographic Computing System JANA2000, Institute of Physics, Academy of Sciences of the Czech Republik, 2000.
9. D. Mercurio, G. Trolliard, T. Hansen, and J. P. Mercurio, *Int. J. Inorg. Mater.* **2**, 397 (2000).
10. V. Petricek, A. Van der Lee, and M. Evain, *Acta Crystallogr. A* **51**, 529 (1995).
11. A. D. Rae, J. G. Thompson, R. L. Withers, and A. C. Willis, *Acta Crystallogr. B* **46**, 474 (1990).
12. C. H. Hervoches and P. Lightfoot, *Chem. Mater.* **11**, 3359 (1999).
13. J. G. Thompson, A. D. Rae, R. L. Withers, and D. C. Craig, *Acta Crystallogr. B* **47**, 174 (1991).